Chemical Engineering Research and Design 205 (2024) 498–509

Contents lists available at ScienceDirect

Chemical Engineering Research and Design

journal homepage: www.elsevier.com/locate/cherd

A CFD study on the change of scale of non-Newtonian stirred digesters at low Reynolds numbers

Francesco Maluta [a,*], Federico Alberini [a], Alessandro Paglianti [a,b], Giuseppina Montante [a]

[a] Department of Industrial Chemistry "Toso Montanari" – Alma Mater Studiorum Università di Bologna, Italy
[b] Interdepartmental Centre for Industrial Agrofood Research – Alma Mater Studiorum Università di Bologna, Italy

ARTICLE INFO

Keywords:
Anaerobic digester
Scale-up
CFD
Laminar regime
Transitional regime

ABSTRACT

Biogas from anaerobic digestion of agricultural waste is proving to be a convincing way to reduce greenhouse gas emissions. To optimize the process energy efficiency, the CFD simulation of the laminar non-Newtonian fluid mixing in the digester would be an effective method, but the adoption of appropriate spatial discretization at the production scale is currently impossible. For this reason, the identification of change of scale rules for an effective design and for preliminary laboratory scale experimental investigations is still of paramount importance. This work is aimed at the identification of a methodology for the scale down of an industrial stirred anaerobic digester with a volume of 1500 m^3, for which CFD simulations have an unacceptable computational cost. The investigation is based on the simulation of three different scale down geometries. The different blade rotational speeds were determined from four different change of scale approaches, which enforced constant blade tip speed, constant shear rate close to the blades, constant Reynolds number and constant power per unit volume, across the different digester sizes. The volume distributions of velocity magnitude, shear rate and shear stress can be exploited to assess the presence of dead zones or localized region where biogas production may be inhibited. The effect of the different change of scale rules on the local instantaneous fluid dynamics were quantified and discussed, finding that both the non-dimensional velocity and non-dimensional shear rate fields are constant across the different scales, when the Reynolds number, based on the Metzner and Otto concept, is constant.

1. Introduction

The demand for green and renewable energy has recently grown remarkably, and biogas from anaerobic digestion attracted attention as a sustainable tool to reduce greenhouse gases emissions. In fact, the biogas is produced from organic waste, and it can be used for heat, power, combined heat and power generation (CHP), and compressed natural gas (CNG) applications (Holm-Nielsen et al., 2009). Agricultural wastes, municipal solid waste, sludge from wastewater treatment and waste from animal farms are suitable feedstocks for anaerobic digestion, mostly owning to their high moisture content (Naqi et al., 2019). The digestate often needs continuous agitation to prevent possible sedimentation and or flotation of the solid fraction (Lebranchu et al., 2017) and the current design of digesters struggles to cope with the wide variety of residues which affect the feedstock and the digestate chemical and physical characteristics (Theuerl et al., 2019). Moreover, the complex composition of the digestate often leads to non-Newtonian rheology and high local viscosity which contribute to making mixing the highest source of power consumption in biogas plants (Kowalczyk et al., 2013). In fact, at the same rotational speed, impellers in laminar regime draw substantially higher power than in turbulent regime and when mixers are operated at low rotational speeds, the torque on the shaft increases considerably, producing high investment costs (Hemrajani and Tatterson, 2004). The key role of mixing on the biogas production in anaerobic digesters is nowadays fully recognized (Li et al., 2022; Schmidell et al., 1986) and process optimization focuses not only on increasing biogas production, but also on reducing the energy demand associated to mixing (Lindmark et al., 2014).

One of the aspects limiting the optimization, control, and design of the anaerobic digestion process is the accuracy of the current modelling development, which cannot satisfactorily describe the entire process in its real complexity (Theuerl et al., 2019). Therefore, the modeling effort is directed on improving both the characterization of the biochemical process chain, and the mechanisms of response of microbiomes to the change in process conditions, and particularly to mixing conditions (Lebranchu et al., 2017; Theuerl et al., 2019). For instance, high

* Corresponding author.
E-mail address: francesco.maluta@unibo.it (F. Maluta).

https://doi.org/10.1016/j.cherd.2024.04.018
Received 7 December 2023; Received in revised form 25 March 2024; Accepted 10 April 2024
Available online 16 April 2024

agitation can lead to disruption of the microbial communities due to excessive stress (Kariyama et al., 2018), while insufficient mixing may reduce the substrate contact with the microbial communities, by fostering the substrate particles segregation from the liquid, limiting the microorganism growth (Karaeva and Khalitova, 2015). The intrinsic coupling between the digester fluid dynamics and the microbial biochemistry makes, as of today, the comprehensive modelling of industrial scale systems prohibitively complex. For this reason, the detailed modelling of the digester flow field is performed in the context of a computational fluid dynamics (CFD) approach, but its applications are mostly limited to the analysis of flow patterns during mixing (Wang et al., 2018). Other modelling approaches rely on more accurate descriptions of the biological pathways, coupled with simplified modelling approaches of the reactor hydrodynamics (Morchain, 2017; Morchain et al., 2013; Pigou and Morchain, 2015). Few studies attempted to couple microbiology to mixing employing a combination of experimental and numerical methods, discussing the experimentally measured biogas production rates in light of the flow field data obtained through CFD simulations (Lebranchu et al., 2017; Sindall et al., 2013). Recently, some examples of simultaneous coupling between fluid dynamics and biokinetics were proposed, but due to the large difference between the characteristic time scales of the two phenomena, either completely segregated solutions (Miana et al., 2023) or solution procedures based on the alternate solution of fluid flow and the biokinetic (Dabiri et al., 2023; Sánchez et al., 2018) were possible.

These studies, that represent a step forward towards the comprehensive modelling of anaerobic digesters, are mostly performed on lab and pilot scale digesters. Limitations on the size of the computational grid inhibit the application of CFD simulations to the production volume and for this reason robust change of scale rules are necessary to extend and compare their results either to larger industrial digester scales, or smaller controlled fermentation environments (Wei et al., 2019). In fact, the complex digestate rheology, which is dependent on the local shear rate, and the stirrer speed and size greatly affect the characteristic time needed to homogenize fresh substrates and additive injections, and few reliable correlations for design and scale-up exist in literature (Kolano et al., 2021). To avoid reductions in the biogas production rate, the maximum shear stress in the digester volume was identified as a fundamental design parameter (Lebranchu et al., 2017) but no stirred digesters change of scale criteria are available for non-Newtonian fluids in laminar regime (Paul et al., 2004). Improvements in the optimization, control, and design of the anaerobic digestion process can be expected from the development of robust methodologies for extending the lab-scale results to the production scale, where the mixing is often insufficient (Capela et al., 2009; Wei et al., 2019). Change of scale rules are fundamental not only in the passage from bench to industrial scale, but also in the opposite change of scale from industrial to lab scale, where the troubleshooting and changes towards process intensification can be more easily tested and implemented (Van Gerven and Stankiewicz, 2009). To this end, a paradigm shift for bioreactor design from the perspective of the large-scale and then step down the scale is encouraged by Noorman, (2011).

This work analyses the effect on the non-Newtonian laminar and early transitional fluid dynamics of different criteria for the change of scale of digesters, with a CFD approach. The manuscript first presents the existing industrial anaerobic digester geometry and the different change of scale rules, then the computational model is presented. Successively, the numerical aspects of the simulations are analysed and discussed to highlight the robustness of the method. A novel method to predict the Metzner-Otto constant for estimating the shear rate from the numerically predicted power consumption is presented, followed by the analysis of the effect of the different change of scale rules on the velocity, shear rate and shear stress distributions, and on the local analysis of velocity and shear rate profiles. Lastly, conclusions are drawn.

2. The system and the change of scale rules

Three scale-down geometries of a 1500 m^3 industrial digester were studied in this work. The industrial 17 m diameter cylindrical vessel was scaled down by 97%, 94% and 69%, corresponding to tank diameters, T, of 0.49 m (T49), 0.98 m (T98) and 5.30 m (T530) respectively. The scale down was performed enforcing geometrical similarity, leading to a liquid height equal to 0.43 T, for each geometry. Each vessel is equipped with three shafts with six blades with a swept diameter equal to D=0.17 T. The three bottom blades of each shaft are inclined at +45° with respect to the horizontal plane, providing up-pumping agitation, while the top three are inclined at −45°, resulting in down-pumping agitation. The stirred tank geometry is reported in Fig. 1, and the T49 geometry was experimentally characterized by Alberini et al., (2023)

The rheology of a sample of the industrial digestate was measured and it was found to follow the Ostwald-de-Waele constitutive equation:

$$\sigma = k_s \dot{\gamma}^n \tag{1}$$

Where σ is the shear stress, $\dot{\gamma}$ is the shear rate, k_s is the consistency index equal to 63.56 Pa·s^n, n is the flow behavior index equal to 0.28, as it can be observed in Fig. 2 where the experimental data, obtained by means of a Anton Paar MCR92 rheometer, are shown together with the regressed curve obtained from Eq. (1).

The density of the digestate, ρ, was also measured and it is equal to 980 kg/m^3. Both the digestate density and rheology were measured at 40°C, which is the temperature at which the industrial digestion runs.

Four different scale down rules were tested to obtain the impeller rotational speeds, N, of the studied tanks: the scale down at constant tip speed, U_{tip}, at constant shear rate close to the blades, at constant Reynolds number, Re, and at constant power per unit volume, P/V. In the following the scale change rules are presented and discussed.

The industrial digester has a blade swept diameter $D_I = 2.93$m and the rotational speed is $N_I = 10.5$rpm. From the definition of $U_{tip} = \pi ND$ it follows that the blade rotational speed of the scale down geometries with blade swept diameter equal to D can be calculated as:

$$N = N_I \left(\frac{D_I}{D}\right) \tag{2}$$

The shear rate of Newtonian and non-Newtonian fluids close to the impeller blades of a Rushton impeller with Reynolds number between 1 and 10000 was correlated with the following expression (Wichterle et al., 1984):

$$\dot{\gamma} = (1 + 5.3n)^{\frac{1}{n}} Re_m^{\frac{1}{1+n}} N \tag{3}$$

Where the modified Reynolds number, Re_m, defined by the authors of Eq. (3) reads as:

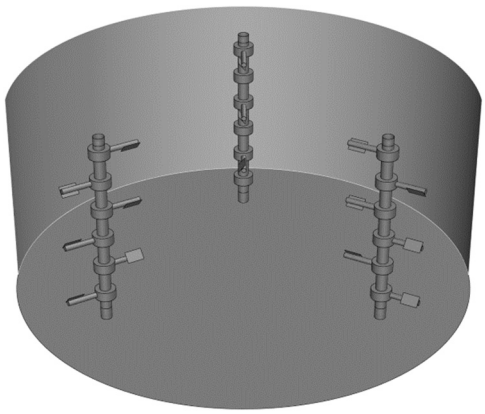

Fig. 1. Stirred tank geometry.

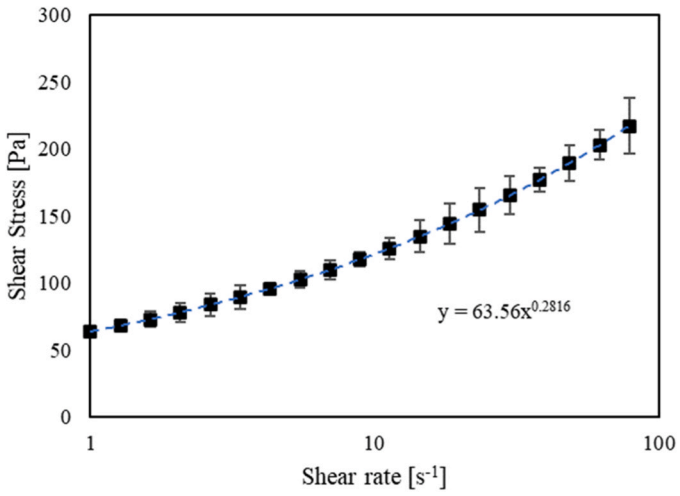

Fig. 2. Experimentally measured shear stress as a function of the shear rate. Black squares are the experimental measurements, error bars are obtained from the standard deviation of the triplicate measurements, and the blue dashed line is the regressed curve obtained from Eq. (1)., which equation is reported below the curve.

$$Re_m = \frac{\rho N^{2-n} D^2}{k_s} \tag{4}$$

From Eq. (3) it follows that the blade rotational speed of the scale downs can be obtained as:

$$N = N_I \left(\frac{D_I}{D}\right)^{\frac{2}{3}} \tag{5}$$

According to Metzner and Otto, (1957) the shear rate is proportional to the impeller speed with the so-called Metzner-Otto constant, K_{MO}, as the constant of proportionality. Following this approach, the Reynolds number based on the apparent viscosity, μ_a, can be obtained as:

$$\mathrm{Re} = \frac{\rho N D^2}{\mu_a} = \frac{\rho N D^2}{k_s (K_{MO} N)^{n-1}} = \frac{\rho N^{2-n} D^2}{k_s K_{MO}{}^{n-1}} \tag{6}$$

Which is slightly different from the Reynolds number in Eq. (4) defined by Wichterle et al. (1984).

Eq. (7) is adopted to obtain the blade rotational speed of the scale down geometry at constant Reynolds number, which reads as:

$$N = N_I \left(\frac{D_I}{D}\right)^{\frac{2}{2-n}} \tag{7}$$

Where it was hypothesized that K_{MO} does not vary with the size change.

The impeller power consumption, P, is expressed in non-dimensional terms by the impeller power number (Hemrajani and Tatterson, 2004), which for stirred tanks it is defined as:

$$Np = \frac{P}{\rho N^3 D^5} \tag{8}$$

In the laminar regime Np is known to be proportional to the inverse of the Reynolds number and it can be obtained as:

$$Np = \frac{C}{\mathrm{Re}} \tag{9}$$

Where C is a parameter which value depends on the type of impeller. Substituting Eq. (9) in Eq. (8), expressing the tank volume as a function of D^3, and computing Re with Eq. (6), the blade rotational speed for a scale down keeping the power per unit volume constant between the different scales can be obtained from Eq. (10) as:

$$N = N_I \tag{10}$$

Where it is highlighted that the dependency on the tank diameter cancels out.

The blade rotational speed obtained with the different scale down rules can be generally expressed as:

$$N = N_I \left(\frac{D_I}{D}\right)^m \tag{11}$$

Where the coefficient m assumes different values, depending on the change of scale rule. In Table 1 the blade rotational speeds obtained with the different scale down rules for the three different geometries considered in this work are reported. Table 1 also shows the corresponding Reynolds numbers calculated with Eq. (6) and with a Metzner-Otto constant equal to 11, as assumed in a previous work (Alberini et al., 2023).

3. The CFD method

The preliminary evaluation of the stirred tank Reynolds numbers presented in Table 1 suggests that the digester works in laminar regime with all the change of scale rules considered, therefore the digestate flow field inside the stirred tanks can be calculated from the direct solution of the mass and momentum conservation equations. Since to obtain the Reynolds number, in a preliminary step, the value of the Metzner-Otto constant was assumed from the literature, the actual value of the constant is determined in Section 4.2, where the hypothesis of laminar regime is also proved. The unsteady, incompressible, isothermal Navier-Stokes equations, Eq. (12) and Eq. (13), solved in this work by the finite volume CFD code ANSYS FLUENT 2021 R1, read as:

$$\nabla \cdot U = 0 \tag{12}$$

$$\rho \frac{\partial U}{\partial t} + \nabla \cdot (\rho U U) = \nabla \cdot \sigma - \nabla P \tag{13}$$

Where U is the velocity vector of the digestate and P is the pressure. The shear stress is calculated from the velocity gradient as:

$$\sigma = \mu_a \left(\nabla U + \nabla U^T\right) \tag{14}$$

Where the term between brackets is the shear rate:

$$\dot{\gamma} = \left(\nabla U + \nabla U^T\right) \tag{15}$$

The rotation of the blades was achieved through the definition of three rotating reference frames, enclosing the shafts and blades, coupled with the steady domain through the sliding mesh approach. In fact, in unbaffled tanks stirred with eccentric shafts the steady-state approximations cannot reproduce the interactions between the impeller jet and

Table 1
Blade rotational speed and Reynolds numbers of the industrial and scale down stirred tanks obtained with different change of scale rules.

Scale	N (rpm)	Re – Eq. (6)	Scale down rule	m
Industrial	10.5	37.3	-	-
T49	366	13.7	Constant U_{tip}	1
T98	183	16.7		
T530	34	26.9		
T49	112	1.8	Constant $\dot{\gamma}$	2/3
T98	71	3.3		
T530	23	13.8		
T49	655	37.3	Constant Re	2/(2-n)
T98	292	37.2		
T530	41	37.2		
T49	10.5	0.03	Constant P/V	0
T98	10.5	0.1		
T530	10.5	3.6		

the stationary walls (Montante et al., 2006). Eqs. (12) and (13) were numerically solved in three domains matching the digester sizes T49, T98 and T530. No-slip boundary conditions were considered on all the solid surfaces of the system, including the top surface. A grid sensitivity study was performed on the T49 geometry to identify the discretization resolution needed to obtain grid independent data. Three grids were built with increasing maximum resolution in the rotating reference frames equal to 1.9 mm for the coarse mesh, 1.5 mm for the intermediate mesh and 1.2 mm for the fine mesh, leading to a total number of cells equal to 1.3 million, 2.4 million and 4.4 million, respectively. Together with the grid sensitivity, a total solution time and a time step sensitivity study were also conducted, and the differences in the predictions were assessed.

Concerning the numerical schemes, the gradients were discretized with the Least Squares Cell Based scheme, pressure interpolation was achieved with a central differencing scheme, convective and diffusive terms were discretized with the second order UPWIND and the central differencing scheme, respectively. Eq. (13) and the pressure-based continuity equation were solved together with a coupled approach. The time discretization was achieved with a second-order implicit discretization scheme with 20 iterations per fixed time step.

Convergence was checked by following the evolution of the local instantaneous velocity on 8 sample points uniformly located on a horizontal line connecting the third blade from the bottom of two different shafts. The position of the point probes is reported in Table 2, where the origin of the axis is located in the geometrical centre of the bottom of the tank.

Moreover, the time evolution of the power, P, calculated from the torque, Γ, on the fixed walls, Eq. (16), and from the volume, V, integral of the mean flow power dissipation, Eq. (17), was monitored.

$$P = 2\pi N\Gamma \tag{16}$$

$$P = \int_V \mu_a \dot{\gamma}\dot{\gamma} dV \tag{17}$$

Convergence was assumed once the monitored variables averaged on a full blade revolution did not change with respect to the previous revolution. The normalized residuals of the x, y, z velocity components and of the pressure-based continuity equation at the beginning of a new time step were always lower than 2×10^{-4}.

4. Results

In this section the simulation results are presented. Firstly, the results of a preliminary verification of the numerical accuracy in the solution of the non-Newtonian fluid flow conservation equations are presented. Successively, the power consumption curve at low Reynolds numbers has been obtained by a set of simulations with Newtonian fluids. Combining the power consumption curve and the power numbers obtained from the simulations with the non-Newtonian fluid in different scales and with different scale down rules, the correct value of the Metzner-Otto constant for the analysed digester is finally obtained. Then, the distributions of the industrial digestate velocity, shear rate and shear stress in the digesters volume are compared with some threshold values proposed in the literature to assess the digester performance, and the effect of the scale and of the change of scale rules on the results are discussed. Lastly, local profiles of the industrial digestate velocity and the shear stress fields are presented and discussed.

Table 2
Dimensionless position of the point probes adopted to check convergence. The axis origin is located on the centre of the tank bottom.

Probe Name	x/T	y/T	z/T
Probe 1	-0.259	-0.112	0.195
Probe 2	-0.227	-0.056	0.195
Probe 3	-0.194	0.000	0.195
Probe 4	-0.162	0.056	0.195
Probe 5	-0.130	0.112	0.195
Probe 6	-0.097	0.168	0.195
Probe 7	-0.065	0.224	0.195
Probe 8	-0.032	0.281	0.195

4.1. Analysis of the numerical accuracy

The effect of the spatial discretization of the computational domain, the size of the time step, the total simulation time, and the number of full blade revolutions on the results are assessed. The T49 digester scale was selected for this analysis, with a blade rotational speed equal to 366 rpm, corresponding to a scale down rule at constant U_{tip} and a Reynolds number of 13.7, Table 1. For the simulations, the industrial digestate was adopted, which properties are reported in Section 2, namely a density equal to 980 kg/m^3, and the fluid rheology determined by Eq. (1). Unless stated differently, average results obtained over one complete impeller revolution are considered. The presented velocity profiles are collected on a horizontal plane at an axial elevation of z = 0.0305 m, thus passing through the lowest blades, and along straight lines obtained at constant coordinates y = −0.084 m and x = −0.149 m, with the axis origin positioned in the centre of the bottom of the tank. A sketch of the measurement plane with the lines along which the velocity profiles are collected is reported in Fig. 3, where the non-dimensional average velocity magnitude obtained with the intermediate mesh is also reported.

The velocity magnitude map in Fig. 3 and the velocity magnitude profiles presented in Fig. 4 are averaged on a time window of 0.164 s, corresponding to a single blade revolution, collected after 0.656 s of solution (4 full blade revolutions) starting from the initial conditions of still fluid and they are obtained with a time step of 2.28 ms, corresponding to a 5° rotation of the blades.

Fig. 4 shows the average velocity magnitude profiles divided by U_{tip} along the lines shown in Fig. 3, and it is evident that the profiles predicted with different mesh resolutions are almost perfectly overlapped. In fact, the maximum deviation in the whole plane is found in the proximity of the tip of the blades, where the coarse mesh underpredicts the average velocity magnitude by less than 5%, with respect to the intermediate and fine mesh predictions. Similar trends are observed on the planes passing through the upper blades. Since different scales and different N result in Reynolds numbers higher than the one corresponding to the conditions considered in this analysis of the numerical accuracy, Table 1, the intermediate mesh resolution was adopted, even though the coarse grid seemed sufficient to obtain grid independent results. Thus, the same maximum spatial resolution of 1.5 mm was kept in the rotating frame of the other scales, leading to grids with 4.4 million elements for the T98 scale and 8.5 million cells for the T530 scale, along with the already mentioned T49 scale which had 2.4 million cells. It is

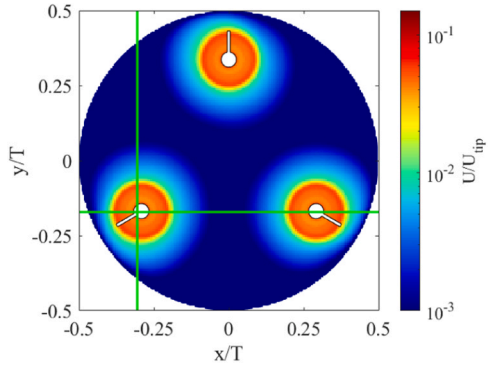

Fig. 3. Average velocity magnitude on a horizontal plane at a non-dimensional axial elevation of z/T = 0.062. The cartesian lines along which the velocity profiles reported hereafter are calculated are reported as straight green lines.

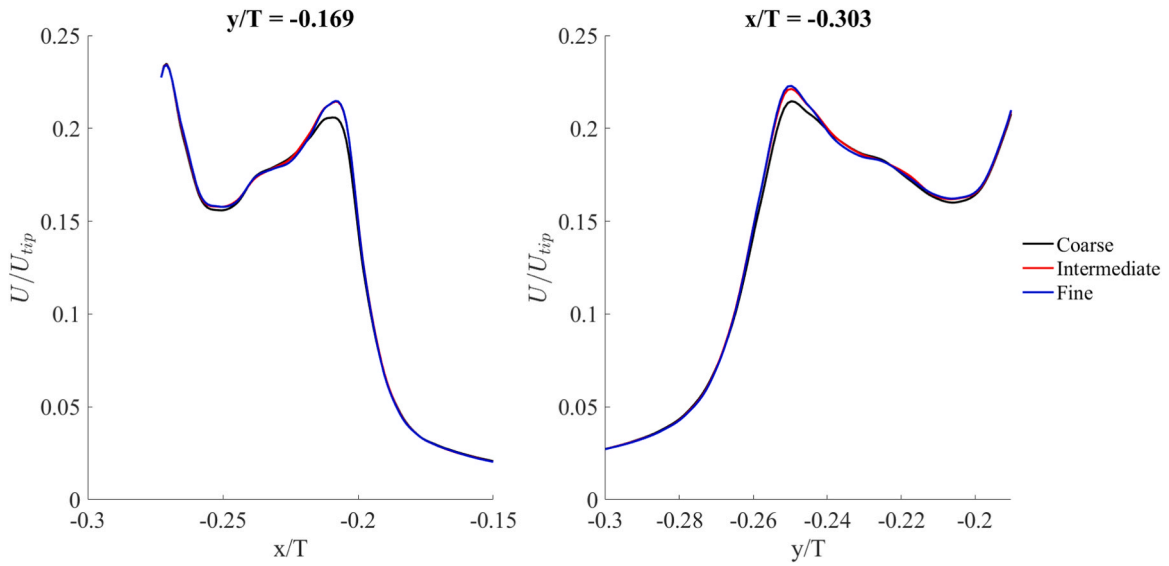

Fig. 4. Non-dimensional average velocity magnitude profiles along the dimensionless x-coordinate, left, and the dimensionless y-coordinate, right, as obtained with the three different meshes, on a horizontal plane passing through the lowest blades.

worth observing that for the discretization of the industrial digester a number of grid elements in the order of hundreds of millions is estimated, which leads to unacceptable computational costs for most applications, both in terms of memory requirements and computational times.

The influence of the time step on the results was also studied. Five different time steps equal to 0.46 ms, 1.37 ms, 2.28 ms, 4.55 ms and 13.66 ms, corresponding to a blade rotation of 1°, 3°, 5°, 10° and 30°, respectively, were adopted to simulate the T49 stirred at N=366 rpm. By means of example, the effect of the different time steps on the power consumption obtained from Eq. (16) and Eq. (17) are reported in Fig. 5.

Fig. 5 shows the percent deviation between the power consumption obtained with the finest time step corresponding to a 1° blade rotation per time step and the same values obtained with longer time steps. Fig. 5 shows that as the time step increases so does the deviation, but while the power consumption obtained from the volume integral of the mean energy dissipation reaches a plateau, the deviation of power consumption obtained from the torque on the fixed walls keeps increasing. With the time step corresponding to a 1° blade rotation, the power consumption calculated with Eq. (16) is equal to 20.1 W, which is almost equal to the value of 20.3 W obtained with Eq. (17). In the following, a

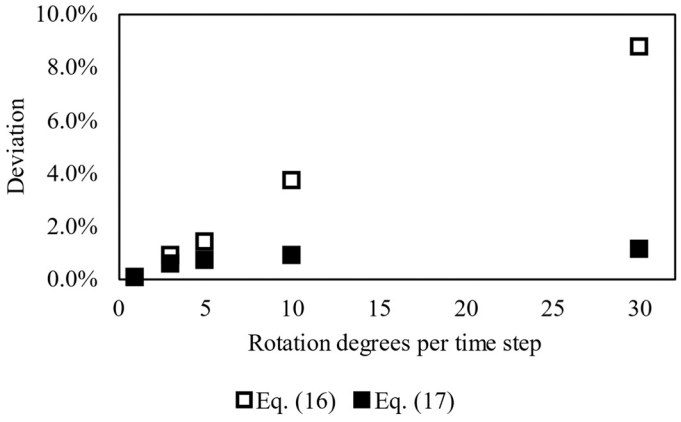

Fig. 5. Power consumption deviation from the value obtained with the finest time step at different time steps. Power consumption are obtained from the torque on fixed walls, Eq. (16) and from the volume integral of the mean energy dissipation, Eq. (17).

time step corresponding to a 5° rotation of the blades was employed, as a compromise between computational time and accuracy. In fact, with such time step the power consumption deviations from the 1° rotation time step values are still below 2% for both the power obtained with Eq. (16) and Eq. (17). For the first method the power consumption is 19.8 W and for the latter is 20.1 W, thus the difference between the two values of the power consumption obtained from Eq. (16) and Eq. (17) is below 2%.

The time needed to obtain the pseudo steady state from the initial conditions of still fluid is shown with the aid of the velocity magnitude obtained on the point probes. A deviation was defined as:

$$\Delta U = \frac{|U_{BP-1} - U_{BP}|}{U_{BP-1}} \tag{18}$$

Where U_{BP} is the velocity magnitude at the probe obtained at a certain blade position during a revolution, and U_{BP-1} is the velocity magnitude at the same probe obtained at the same blade position during the previous revolution. The evolution of ΔU with the increasing number of blades revolution is reported in Fig. 6a.

Fig. 6a confirms that very rapidly the flow field reaches the pseudo steady state, and after four blade revolutions the parameter ΔU reaches an almost constant value which is below 10^{-7}, for all the different probes considered. Similar trends are obtained at different blade rotational speeds, and the same result is confirmed by the analysis of the shear rate and the power consumption. To obtain the average velocity of the digestate, the local velocity field must be averaged at least on a full blade revolution. To determine whether a single revolution is sufficient to have time averaged velocity field independent on the averaging window, the instantaneous velocity magnitude field at the pseudo steady state was averaged on different time windows corresponding to a number of blade revolutions up to 10 after the 4 complete revolutions needed to obtain the pseudo steady state. The averaged velocity magnitude profiles along the line at constant y-coordinate of Fig. 3 are shown by means of example in Fig. 6b. Fig. 6b shows that the average velocity magnitude profiles obtained with different averaging windows produce profiles which are perfectly overlapped. For this reason, in the following the average results are reported on an average window corresponding to one full blade revolution.

Based on the analysis reported in this section, the results of the simulations presented hereafter are obtained with the intermediate mesh resolution and with a time step corresponding to a blade rotation

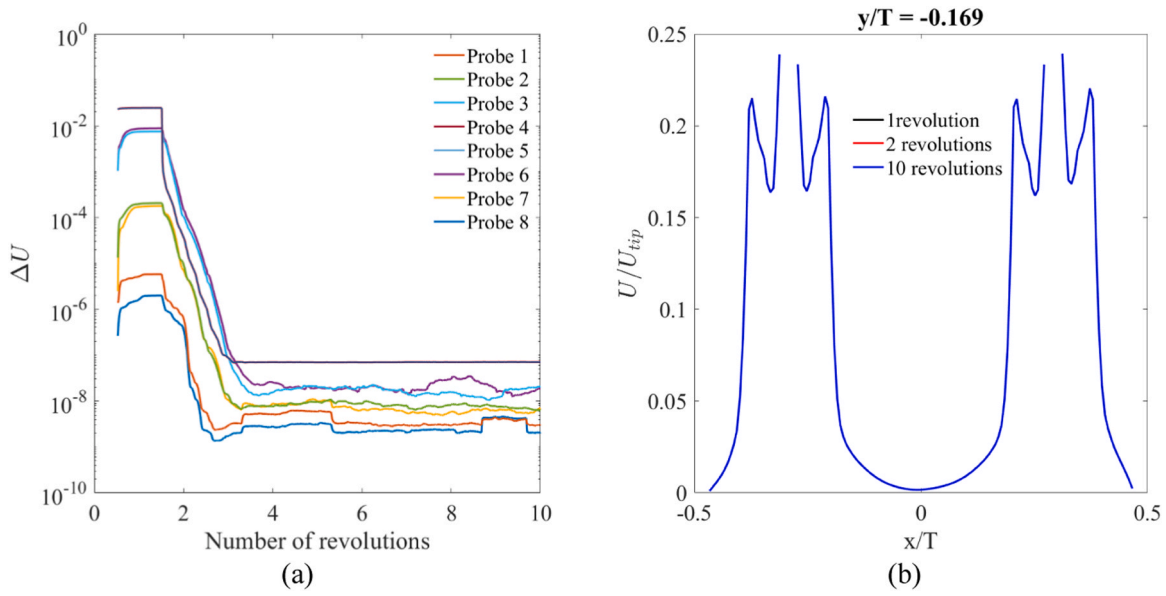

Fig. 6. Evolution of the parameter ΔU with increasing number of revolutions (a). The location of the probes is reported in Table 2. Dimensionless velocity magnitude profiles averaged on different time windows, (b).

of 5°. Results are collected at the pseudo steady state reached after 4 full revolutions of the blades, and time average variables and global parameters are averaged on a time window corresponding to a single blade revolution.

4.2. Power consumption and Metzner-Otto constant determination

As also reported in Section 2, the Metzner-Otto constant, K_{MO}, correlates the shear rate to the blade rotational speed, and it is a function of the impeller type. When this constant is not known a priori the impeller power curve can be exploited to obtain it. In fact, if the power consumption in one or more operative conditions in the laminar regime is known, the impeller power number can be obtained with Eq. (8), and the apparent Reynolds number based on the apparent viscosity can be calculated from Eq. (9). The apparent viscosity is then calculated from the Reynolds number definition, Eq. (6), and if the rheology of the fluid is known, the shear rate can be calculated as:

$$\dot{\gamma} = \left(\frac{\mu_a}{k_s}\right)^{\frac{1}{n-1}} \tag{19}$$

Thus, the Metzner–Otto relationship can be adopted to obtain K_{MO} as:

$$K_{MO} = \frac{\dot{\gamma}}{N} \tag{20}$$

Substituting the relationship chain, K_{MO} can be calculated as follows:

$$K_{MO} = \left(\frac{P}{k_s C N^{n+1} D^3}\right)^{\frac{1}{n-1}} \tag{21}$$

This method was adopted to calculate the Metzner-Otto constant for the stirrer employed in the digester, for which a known value was not available. To do so, the first step was to obtain the power curve in the laminar regime. Since to obtain the apparent Reynolds number of non-Newtonian fluids, Eq. (6), the Metzner-Otto constant must be known, the power curve in the laminar regime was obtained with simulations of Newtonian fluids. Eight simulations in the T49 geometry with N kept constant at 300 rpm were performed with hypothesized Newtonian model fluids of density equal to ρ=980 kg/m^3 and with different constant viscosities. The constant viscosities were assumed to obtain Reynolds numbers spanning from 1 to 100, which is the laminar limit in stirred tanks (Lamberto et al., 1999). The viscosities and the relative Reynolds numbers employed to obtain the power curve in the laminar regime are reported in Table 3.

The power consumption for each simulation was calculated through Eq. (17), and the power curve is reported in Fig. 7, together with the experimental data collected by Alberini et al., (2023).

Fig. 7 shows that the power number decreases linearly with increasing Reynolds numbers up to about 20, where it begins to deviate from the linear approximation, and this may be interpreted as the onset of the transitional regime. The good agreement of the experimental and the computed values of Np up to Re about 100 suggests that the direct solution of the Navier Stokes equations provides realistic predictions also in the very early transitional regime.

From the regression on the numerical data with Re lower than 10, a value of C = 82.4 is found, which is used to calculate the value of the Metzner-Otto constant, together with the power consumption obtained from the simulations of the industrial digestate mixing in different vessel scales and with the different change of scale rules listed in Table 1. The results are summarized in Table 4, and in Fig. 8 the calculated shear rates are plotted against the corresponding N just for those cases with Re lower than 15, in order to limit the analysis to the laminar regime, strictly. Based on the results of Table 4, the expected Reynolds number is lower than 15 for almost all the change of scale rules considered, therefore the hypothesis of laminar regime is proven to hold. Given the agreement of the numerical results with the experiments shown in Fig. 7, with the selected grid resolution a negligible error is expected from the direct numerical solution of Eq.(12) and Eq.(13) at Re slightly above the

Table 3
Viscosities of the fluids and Reynolds numbers employed in the simulations to obtain the power curve in the laminar regime.

μ (Pa.s)	Re
34.574	1
17.287	2
6.915	5
3.457	10
1.729	20
1.152	30
0.691	50
0.346	100

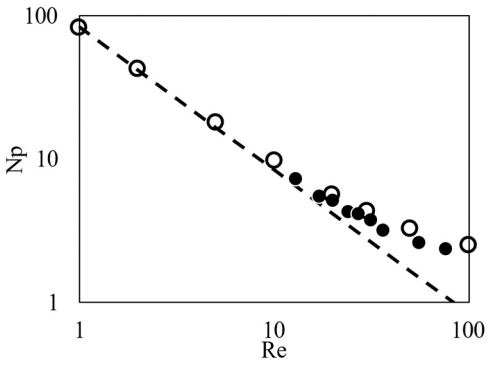

Fig. 7. Power curve obtained through numerical simulations, open circles, and experimental data from (Alberini et al., 2023), solid circles. The dashed line represents Eq. (9), with C regressed from the numerical results.

linear trend of the power curve.

Fig. 8 confirms that a single value of the Metzner-Otto constant can be employed to correlate the shear rates with the blade rotational speeds with reasonable accuracy in the laminar regime. In fact, the regressed value of K_{MO} based on all the data in Fig. 8 is equal to 8.3, with a coefficient of determination of 0.998. To check the robustness of the method, an additional simulation with the rheological properties of a mixture of 6 g/l of CMC in water reported in Alberini et al., (2023) was run in the T49 tank stirred at N=10.5 rpm and Re=1.0. The impeller power consumption calculated with Eq. (17) is equal to 0.002 W and the resulting K_{MO} obtained with Eq.(21) is equal to 8.6. This value overestimates the value obtained from the regression based on the 8 numerical results shown in Fig. 8 by about 3%, while with the value of 11 usually considered for fast impeller the overestimation would have been of 32%. This result highlights the importance of a specific evaluation of the Metzner-Otto constant for unconventional stirred tanks, which can be obtained with the computational approach suggested in this work, while the adoption of literature data obtained in different systems can induce important errors.

4.3. Velocity, shear rate and shear stress distributions

The results presented in this and in the following Sections are obtained with the fluid properties of the non-Newtonian industrial digestate reported in Section 2. According to Vesvikar and Al-Dahhan, (2005) and Bridgeman, (2012), dead or stagnant volume in the digester is defined as those regions where the fluid velocity is less than 5% of the maximum velocity in the digester. The average velocity magnitude distributions in terms of digester volume percent at different scales and with different change of scale rules were calculated, and by means of example the cumulative distribution obtained from the scale down at constant U_{tip} is shown in Fig. 9.

Fig. 9 shows that, according to the proposed definition, in all the three scales considered the dead volume accounts for around 95% of the total digester volume, meaning that the blades manage to move just the small amount of fluid close to the shaft. This may cause long homogenization and recirculation times, as well as the formation of hot spots and substrate/byproduct accumulation, which may damage the microorganisms and trigger different metabolic pathways. Furthermore, no appreciable differences are found in the volume distributions of the velocities higher than 1% of the tip speed, meaning that the change of scale negligibly changes the average fluid flow. Very similar results are

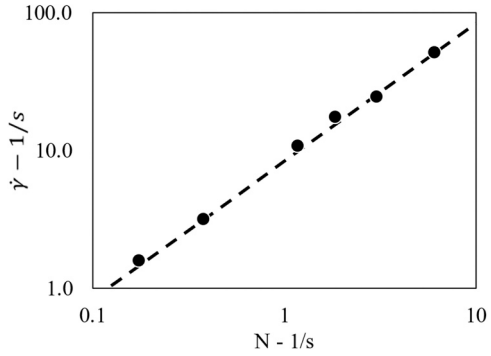

Fig. 8. Shear rates calculated from the numerical power consumptions at different scales and with different change of scale rules, solid circles. Just the cases at Re lower than 15 are considered. The dashed line is obtained from Eq. (20), with K_{MO} regressed from the shown numerical results.

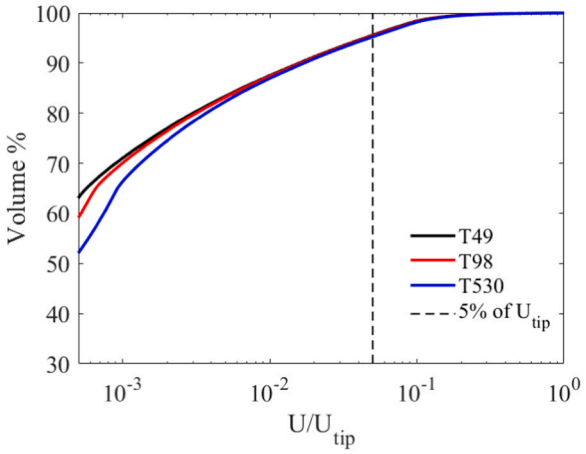

Fig. 9. Average non-dimensional velocity magnitude cumulative distribution in the digester volume as obtained from the simulations at different scales, with N obtained from the change of scale at constant U_{tip}. The threshold to identify the dead zones is reported as a dashed line.

Table 4
Results of the procedure to calculate K_{MO} from the power curve. Cases in bold are not employed in the regression procedure.

Scale down rule	Scale	N (rpm)	P (W)	Np	Re	μ_a (Pa.s)	$\dot{\gamma}$ (1/s)	K_{MO}
Constant U_{tip}	T49	366	20.5	7.2	11.5	3.8	50.7	8.6
	T98	183	69.8	6.1	13.5	6.4	24.2	8.2
	T530	**34**	**1394.6**	**4.2**	**19.7**	**23.8**	**3.9**	**7.2**
Constant $\dot{\gamma}$	T49	112	4.2	50.9	1.6	8.2	17.2	9.5
	T98	71	18.9	28.2	2.9	11.5	10.7	9.3
	T530	23	753.8	7.3	11.4	28.0	3.1	8.4
Constant Re	**T49**	**655**	**54.6**	**3.3**	**24.8**	**3.1**	**65.8**	**6.2**
	T98	**292**	**156.6**	**3.4**	**24.5**	**5.7**	**28.9**	**6.1**
	T530	**41**	**1983.7**	**3.3**	**24.8**	**23.0**	**4.1**	**6.2**
Constant P/V	T49	10.5	0.2	2962.8	0.03	44.9	1.6	9.5
	T98	10.5	1.6	749.3	0.11	45.4	1.6	9.4
	T530	10.5	260.8	26.0	3.2	46.1	1.6	9.2

obtained with the other change of scale rules and are omitted for brevity.

Jiang et al., (2016) reported that shear rate above 5 s^{-1} increased the abrasion of the anaerobic sludge granules, which in turn may negatively affect the biogas production and methane content. Even though such value of the critical shear rate may be dependent on the system and process under consideration (Lebranchu et al., 2017), the numerical simulations may provide a tool to monitor and compare the shear rate in different scales and operative conditions. For these reasons, together with the velocity magnitude distributions, the average shear rate distributions were also calculated, and they are shown in Fig. 10. Fig. 10 shows that increasing the digester scale results in lower $\dot{\gamma}$ intensities. While this may be beneficial to reduce the abrasion of sludge granules, a reduced shear rate leads to higher power consumption and higher apparent viscosities, which affect the size of the mass and energy transfer boundary layers, leading to slower transport rates (Hemrajani and Tatterson, 2004). In the present work, the largest volume percent exceeding the proposed $\dot{\gamma}$ threshold is found for the T49 scaled at constant Re, for which about 14% of the volume has shear rates higher than 5 s^{-1}. Concerning the change of scale rule, scaling down at constant Re leads to the highest $\dot{\gamma}$ and the largest variations between scales, followed by the scale down at constant U_{tip} and then constant $\dot{\gamma}$. It is interesting to notice that with the latter change of scale rule the shear rates in the different scales are not indeed constant. The average shear rate distributions obtained by scaling down at constant power per unit volume are almost perfectly overlapped since the characteristic velocities with this change of scale rule are around one order of magnitude lower than those obtained with the other rules. In fact, the maximum $\dot{\gamma}$ values in the digester volume are lower than 2 s^{-1}.

Unsurprisingly, the trends of the average shear stress distributions follow those of the average shear rate distributions reported in Fig. 10. By means of example, just the cumulative volume distribution of σ obtained with the change of scale rule at constant Re number is reported in

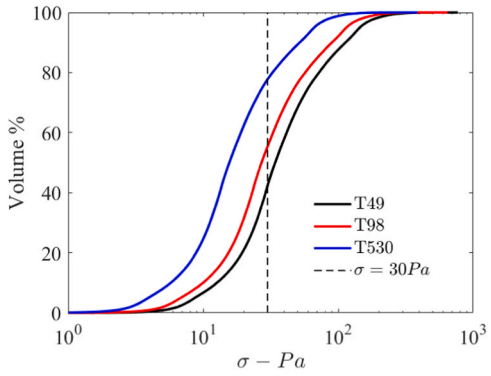

Fig. 11. Average shear stress cumulative distribution in the digester volume as obtained from the simulations at different scales, with N obtained from the change of scale at constant Re. The threshold to identify the limit at which biogas production may be affected is reported as a dashed line.

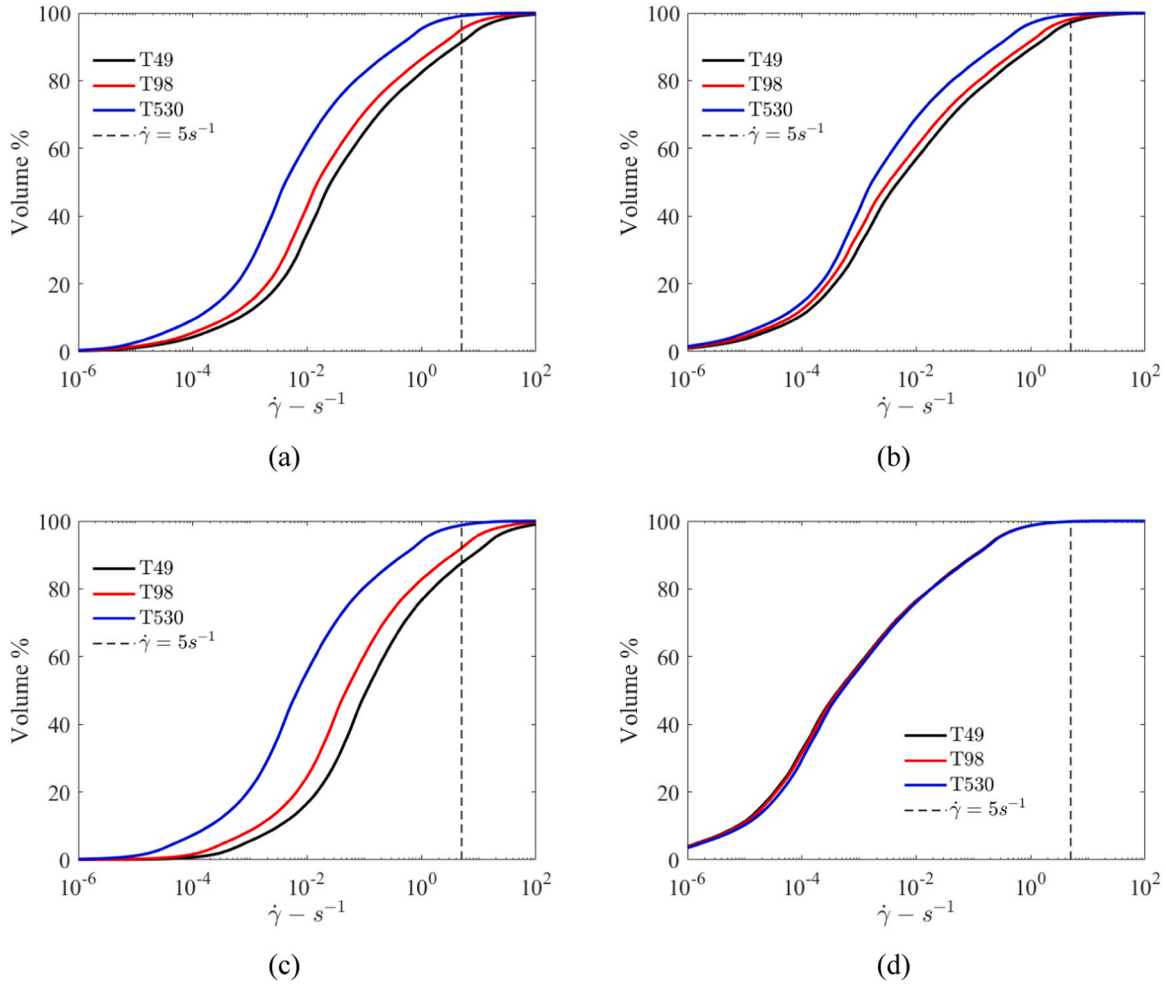

Fig. 10. Average shear rate cumulative distributions in the digester volume as obtained from the simulations at different scales, with N obtained from the change of scale at constant U_{tip}, (a), constant $\dot{\gamma}$, (b), constant Re, (c) and constant P/V, (d). The proposed threshold to identify the limit at which biogas production may be affected is reported as a dashed line.

Fig. 11, since the highest shear stress values are found, together with the highest shear stress variations with the change of scale.

Fig. 11 confirms that the highest stresses are observed at the smallest scale, where the blade rotational speed is the highest. Lebranchu et al., (2017) proved that the maximum shear stress may be used as a guide in the design of digesters to avoid the slow-down of methane production rate, and in their conditions, they found that shear stresses higher than 30 Pa negatively affected the biogas production rate. Although this threshold may not be universal, as reported by the authors, it was plotted in the distributions of Fig. 11 as a possible benchmark to assess the change of scale effects. Increasing the tank diameter, the volume percent where σ exceeds the proposed threshold changes from approximately 58% in the T49 to 21% in the T530. On one hand, the reduction in σ reduces the stress on the microorganisms with a beneficial effect on the biogas production rate, but on the other hand it may affect the particle suspension by reducing the Shields number, θ, which is defined as $\theta = \sigma/g(\rho_p - \rho)d_p$, where g is the gravitational acceleration, ρ_p is the particle density and d_p is its diameter. In fact, Lassaigne et al., (2016) found that the mechanism for solid suspension in the laminar regime may be described as a particle bed erosion, which onset is characterized by a critical Shields number. Depending on the system under consideration, a reduction of the shear stress may lead to Shields numbers below the critical value, with detrimental effects on the solid suspensions and thus on the biogas production rate. With the other change of scale rules, the volume percent where σ exceeds the proposed threshold changes from 39% to 20% by scaling at constant U_{tip} from the T49 to the T530, from 26% to 17% by scaling at constant $\dot{\gamma}$ from the T49 to the T530 and it is around 12% for all the different scales, when the constant P/V rule is adopted.

4.4. Local analysis

The last analysis presented in this work concerns the local analysis of the instantaneous non-dimensional velocity magnitudes and shear rates, which is performed on the horizontal plane passing through the lowest blades, along the lines reported in Fig. 3. Since the shear stress is univocally determined by the shear rate, Eq. (1), the σ profiles are omitted for sake of conciseness. The instantaneous variables are analyzed, for highlighting their peak values. The instantaneous non-dimensional velocity magnitudes obtained on the three different scales with the change of scale at constant Reynolds number are reported in Fig. 12.

Fig. 12 shows that the velocity magnitude profiles divided by the tip speed scale with the Reynolds number. In fact, the profiles almost perfectly overlap, and the small differences may be due to the different number of grid points on which the data are collected. Other sources of uncertainty may be due to the rounding error in obtaining the blade rotational speed from the change of scale rule and the rounding error in the time step, which may have caused slightly different blade positions at the end of the simulations. The other change of scale rules do not produce similar profiles across the different scales, as it can be seen by means of example in the instantaneous non-dimensional velocity magnitudes obtained on the three different scales with the change of scale at constant shear rate reported in Fig. 13.

In fact, the profiles in Fig. 13 not only show that deviations larger than those observable in Fig. 12 are produced, but also that the shape of the profile changes as the scale of the digester is changed. Similar differences are obtained with the change of scale at constant U_{tip} and at constant P/V.

Together with the dimensionless velocity field, also the dimensionless shear rate field scales with the Reynolds number. By means of example, in Fig. 14 the instantaneous shear rates obtained on the three different scales with the change of scale at constant Reynolds number and at constant power per unit volume are reported.

When the shear rates are divided by the blade rotational speed they fall on a single profile, if the change of scale is performed at constant Reynolds number, Fig. 14a. From the analysis of the shear rate distributions in Section 4.3, it seems that the change of scale at constant P/V produced shear rate fields which were similar across the scales. However, the local analysis of the instantaneous profiles, Fig. 14b, shows that in the proximity of the blades different profiles are obtained, both in terms of shear rate intensity and in terms of profile shape.

As a further confirmation, the instantaneous non-dimensional velocity magnitude and shear rate profiles obtained with different change of scale rules but with similar Reynolds numbers are compared in Fig. 15.

In fact, the Reynolds number for the T49 scaled at constant U_{tip}, hence with m=1 in Eq. (11), is equal to 9.5, and that of the T530 scaled at constant $\dot{\gamma}$, m=2/3 in Eq. (11), is equal to 9.6. Moreover, the Reynolds number of the T98 scaled at constant $\dot{\gamma}$ is equal to 2.3, while that of the T530 scaled at constant P/V, m=0 in Eq. (11), is equal to 2.5. The Reynolds numbers were calculated with the Metzner-Otto constant obtained in Section 4.2. Fig. 15 confirms that both the non-dimensional

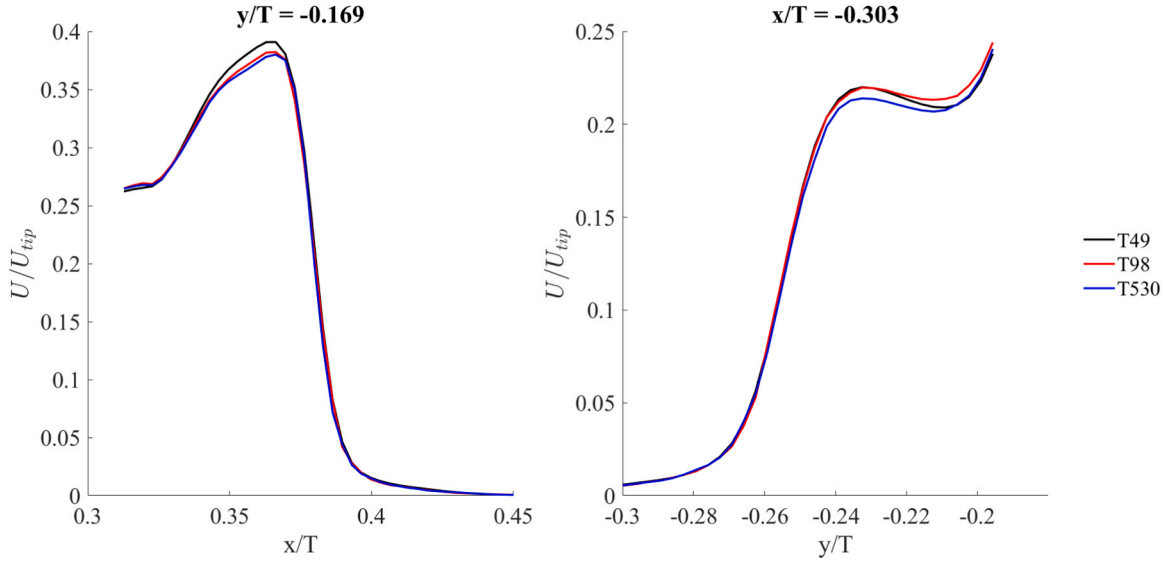

Fig. 12. Instantaneous non-dimensional velocity magnitude profiles along the cartesian coordinates shown in Fig. 3 for the different digester scales obtained with the change of scale at constant Re.

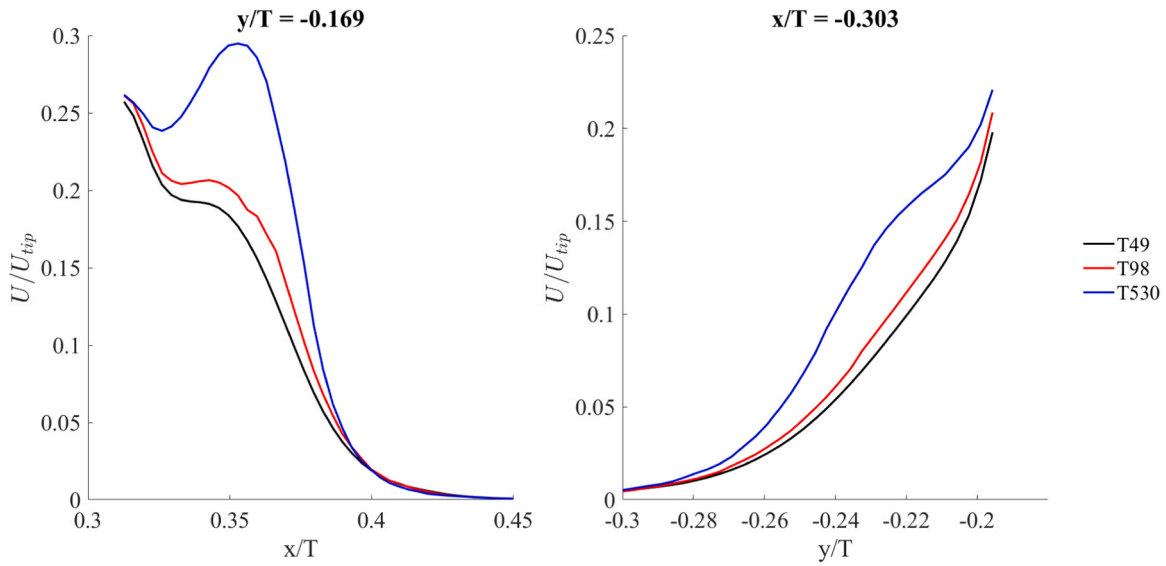

Fig. 13. Instantaneous non-dimensional velocity magnitude profiles along the cartesian coordinates shown in Fig. 3 for the different digester scales obtained with the change of scale at constant $\dot{\gamma}$.

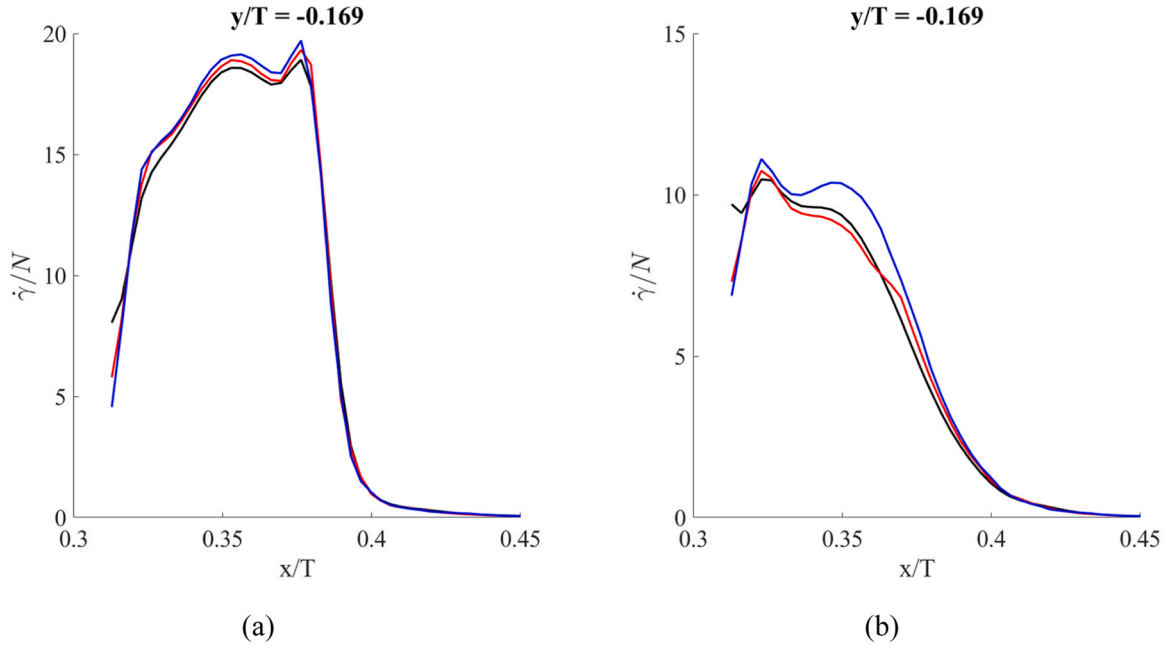

Fig. 14. Instantaneous non-dimensional shear rate profiles along the cartesian coordinates shown in Fig. 3 for the different digester scales obtained with the change of scale at constant Re, (a), and at constant P/V, (b).

velocity magnitude field and the non-dimensional shear rate field scale with the Reynolds number. Therefore, the change of scale rule enforcing the same Reynolds number across the different scales may allow to predict a priori the velocity, the shear rate and the shear stress fields inside stirred tanks operating in the laminar regime. Since the numerical simulation of the industrial scale digester results either in a prohibitively large number of cells in the discretized computational domain, or alternatively in an insufficient spatial resolution, the possibility to infer the non-dimensional velocity and shear rate fields from simulations performed at smaller scales may provide important information while simultaneously reducing the computational cost.

Nonetheless, attention must be paid, since scaling at constant Reynolds number also produces the largest variations of dimensional shear rate and shear stress with the digester scale. In fact, for instance, the shear stress increase may damage the microorganisms during the scale down, while its decrease may lead to suboptimal suspensions during the scale up.

5. Conclusions

Different change of scale rules are presented and their effect on the fluid dynamics of the non-Newtonian digestate in laminar regime inside of three different scale-downs of an industrial stirred digester geometry are analysed with a CFD approach. The numerical requirements of the simulations are studied in terms of grid resolution, time step size, time to reach the pseudo steady state and revolutions upon which averaging the results, and these results may serve as guidelines for the CFD simulations of such stirred digesters working under laminar and early transitional

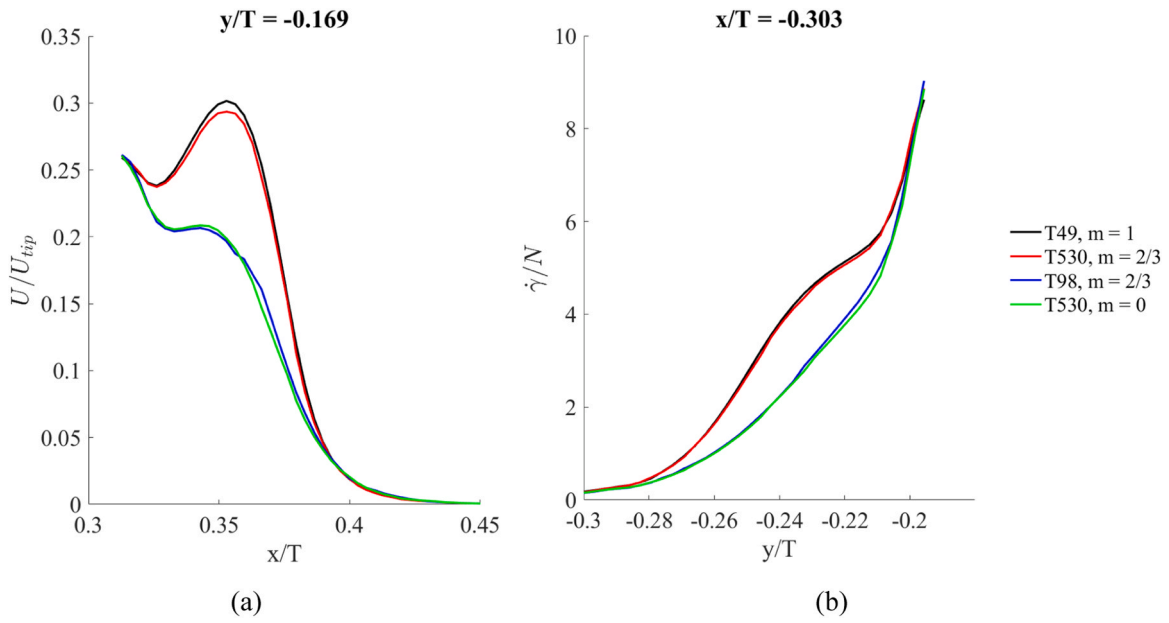

Fig. 15. Instantaneous non-dimensional velocity magnitude, (a), and shear rate, (b), profiles along the cartesian coordinates shown in Fig. 3 for different digester scales and change of scale rules with similar Reynolds numbers.

regimes.

The outcome of the investigation is twofold. The main result is the identification of the change of scale criterion for satisfying specific constraints on critical process variables, e.g. the shear rate, shear stress or the mean velocity. The other important outcome is to gain insight into the fluid-dynamic behaviour of the digester. It is observed that the non-dimensional velocity magnitude and the non-dimensional shear rate scale with the rotational Reynolds number. For the definition of the Reynolds number for the non-Newtonian fluid, an appropriate Metzner-Otto constant is necessary, and the method suggested in this work allows to obtain appropriate values for any geometry. Obviously, the design of the digester based on the CFD simulation of the real size digester would be more accurate than a design based on the analysis of dimensionless numbers, but for thousands of m^3 volume equipment a reliable CFD simulation nowadays is not affordable, due to the huge computational grid size. Therefore, a preliminary analysis based on a simplified approach is necessary.

The Metzner-Otto constant for the blades employed in the digester mixing was calculated with a novel method based on the regression of the shear rate from the power consumption obtained from the simulations in laminar regime, and the procedure can be employed to other stirrers, helping in the design and the change of scale of different geometries. The computational approach can be adopted to obtain information on the volumetric distribution of dead zones, shear rates and stresses, aiding in controlling the digester operations and both allowing an a priori evaluation of the digester characteristics, and providing a tool to quantify the digester volume fraction working in critical conditions. The local analysis of the velocity magnitude and shear rate profiles revealed that performing a change of scale based on the Reynolds number, obtained assuming a single value of the Metzner-Otto constant, produces scale invariant fields of non-dimensional velocity magnitude and non-dimensional shear rate. It follows that the velocity, shear rate and shear stress non-dimensional fields at the industrial scale can be determined from smaller scales, saving computational resources, and simplifying the experimental characterization. On the other hand, the change of scale rule at constant Reynolds number results in the largest differences in the dimensional shear rate and shear stress with the digester size, with respect to the other change of scale rules considered.

CRediT authorship contribution statement

Giuseppina Montante: Conceptualization, Methodology, Supervision, Writing – original draft. **Alessandro Paglianti:** Conceptualization, Funding acquisition, Supervision, Writing – original draft. **Federico Alberini:** Investigation, Validation, Writing – review & editing. **Francesco Maluta:** Investigation, Methodology, Software, Writing – original draft.

Declaration of Competing Interest

The authors declare that they have no known competing financial interests or personal relationships that could have appeared to influence the work reported in this paper

Acknowledgment

This work was partially financially supported under the Agritech National Research Center and received funding from the European Union Next-Generation EU (PIANO NAZIONALE DI RIPRESA E RESILIENZA (PNRR) – MISSIONE 4 COMPONENTE 2, INVESTIMENTO 1.4 – D.D. 1032 17/06/2022, CN00000022)”

References

Alberini, F., Maluta, F., Paglianti, A., Montante, G., 2023. Power consumption and fluid mixing in a scale-down geometry of a stirred digester for biogas production. ACS Eng. Au 3, 102–113. https://doi.org/10.1021/acsengineeringau.2c00047.

Bridgeman, J., 2012. Computational fluid dynamics modelling of sewage sludge mixing in an anaerobic digester. Adv. Eng. Softw. 44, 54–62. https://doi.org/10.1016/j.advengsoft.2011.05.037.

Capela, I., Bilé, M.J., Silva, F., Nadais, H., Prates, A., Arroja, L., 2009. Hydrodynamic behaviour of a full-scale anaerobic contact reactor using residence time distribution technique. J. Chem. Technol. Biotechnol. 84, 716–724. https://doi.org/10.1002/jctb.2104.

Dabiri, S., Kumar, P., Rauch, W., 2023. Integrating biokinetics with computational fluid dynamics for energy performance analysis in anaerobic digestion. Bioresour. Technol. 373, 128728 https://doi.org/10.1016/j.biortech.2023.128728.

Hemrajani, R.R., Tatterson, G.B., 2004. MECHANICALLY STIRRED VESSELS. In: Paul, E. L., Atiemo-Obeng, V.A., Kresta, S.M. (Eds.), HANDBOOK OF INDUSTRIAL MIXING Science and Practice. John Wiley & Sons Inc, Hoboken, New Jersey, USA, pp. 345–389.

Holm-Nielsen, J.B., Al Seadi, T., Oleskowicz-Popiel, P., 2009. The future of anaerobic digestion and biogas utilization. Bioresour. Technol. 100, 5478–5484. https://doi.org/10.1016/j.biortech.2008.12.046.

Jiang, J., Wu, J., Poncin, S., Li, H.Z., 2016. Effect of hydrodynamic shear on biogas production and granule characteristics in a continuous stirred tank reactor. Process Biochem. 51, 345–351. https://doi.org/10.1016/j.procbio.2015.12.014.

Karaeva, J.V., Khalitova, G.R., 2015. Evaluation of mixing quality in anaerobic digester. J. Renew. Sustain. Energy 7. https://doi.org/10.1063/1.4923327.

Kariyama, I.D., Zhai, X., Wu, B., 2018. Influence of mixing on anaerobic digestion efficiency in stirred tank digesters: A review. Water Res 143, 503–517. https://doi.org/10.1016/j.watres.2018.06.065.

Kolano, M., Danke, J., Kraume, M., 2021. Using thrust to control the mixing process in stirred tanks with side-entering agitators and viscoelastic fluids. Biomass-.-. Bioenergy 152, 106180. https://doi.org/10.1016/j.biombioe.2021.106180.

Kowalczyk, A., Harnisch, E., Schwede, S., Gerber, M., Span, R., 2013. Different mixing modes for biogas plants using energy crops. Appl. Energy 112, 465–472. https://doi.org/10.1016/j.apenergy.2013.03.065.

Lamberto, D.J., Alvarez, M.M., Muzzio, F.J., 1999. Experimental and computational investigation of the laminar flow structure in a stirred tank. Chem. Eng. Sci. 54, 919–942. https://doi.org/10.1016/S0009-2509(98)00275-9.

Lassaigne, M., Blais, B., Fradette, L., Bertrand, F., 2016. Experimental investigation of the mixing of viscous liquids and non-dilute concentrations of particles in a stirred tank. Chem. Eng. Res. Des. 108, 55–68. https://doi.org/10.1016/j.cherd.2016.01.005.

Lebranchu, A., Delaunay, S., Marchal, P., Blanchard, F., Pacaud, S., Fick, M., Olmos, E., 2017. Impact of shear stress and impeller design on the production of biogas in anaerobic digesters. Bioresour. Technol. 245, 1139–1147. https://doi.org/10.1016/j.biortech.2017.07.113.

Li, L., Wang, K., Zhao, Q., Gao, Q., Zhou, H., Jiang, J., Mei, W., 2022. A critical review of experimental and CFD techniques to characterize the mixing performance of anaerobic digesters for biogas production. Rev. Environ. Sci. Biotechnol. 21, 665–689. https://doi.org/10.1007/s11157-022-09626-z.

Lindmark, J., Thorin, E., Bel Fdhila, R., Dahlquist, E., 2014. Effects of mixing on the result of anaerobic digestion: Review. Renew. Sustain. Energy Rev. 40, 1030–1047. https://doi.org/10.1016/j.rser.2014.07.182.

Metzner, A.B., Otto, R.E., 1957. Agitation of non-Newtonian fluids. AIChE J. 3, 3–10. https://doi.org/10.1002/aic.690030103.

Miana, M., Santamaría, A.M., Carbajo, J.B., Bengoechea, C., García, G., Izquierdo, S., 2023. A Practical Approach for Biochemical Modeling in the CFD Evaluation of Novel Anaerobic Digester Concepts for Biogas Production. Processes 11, 2851. https://doi.org/10.3390/pr11102851.

Montante, G., Bakker, A., Paglianti, A., Magelli, F., 2006. Effect of the shaft eccentricity on the hydrodynamics of unbaffled stirred tanks. Chem. Eng. Sci. 61, 2807–2814. https://doi.org/10.1016/j.ces.2005.09.021.

Morchain, J., 2017. Bioreactor Modeling: Interactions between Hydrodynamics and Biology. ISTE Press Ltd/Elsevier Ltd, London/Oxford.

Morchain, J., Gabelle, J.C., Cockx, A., 2013. Coupling of biokinetic and population balance models to account for biological heterogeneity in bioreactors. AIChE J. 59, 369–379. https://doi.org/10.1002/aic.13820.

Naqi, A., Kuhn, J.N., Joseph, B., 2019. Techno-economic analysis of producing liquid fuels from biomass via anaerobic digestion and thermochemical conversion. Biomass-.-. Bioenergy 130, 105395. https://doi.org/10.1016/j.biombioe.2019.105395.

Noorman, H., 2011. An industrial perspective on bioreactor scale-down: What we can learn from combined large-scale bioprocess and model fluid studies. Biotechnol. J. 6, 934–943. https://doi.org/10.1002/biot.201000406.

Paul, E.L., Atiemo-obeng, V. a, Kresta, S.M., 2004. HANDBOOK OF INDUSTRIAL MIXING Edited by. https://doi.org/10.1002/0471451452.

Pigou, M., Morchain, J., 2015. Investigating the interactions between physical and biological heterogeneities in bioreactors using compartment, population balance and metabolic models. Chem. Eng. Sci. 126, 267–282. https://doi.org/10.1016/j.ces.2014.11.035.

Sánchez, F., Rey, H., Viedma, A., Nicolás-Pérez, F., Kaiser, A.S., Martínez, M., 2018. CFD simulation of fluid dynamic and biokinetic processes within activated sludge reactors under intermittent aeration regime. Water Res 139, 47–57. https://doi.org/10.1016/j.watres.2018.03.067.

Schmidell, W., Craveiro, A.M., Peres, C.S., Hirata, Y.S., Varella, R.F., 1986. Anaerobic Digestion of Municipal Solid Wastes. Water Sci. Technol. 18, 163–175. https://doi.org/10.2166/wst.1986.0172.

Sindall, R., Bridgeman, J., Carliell-Marquet, C., 2013. Velocity gradient as a tool to characterise the link between mixing and biogas production in anaerobic waste digesters. Water Sci. Technol. 67, 2800–2806. https://doi.org/10.2166/wst.2013.206.

Theuerl, S., Herrmann, C., Heiermann, M., Grundmann, P., Landwehr, N., Kreidenweis, U., Prochnow, A., 2019. The Future Agricultural Biogas Plant in Germany: A Vision. Energ. (Basel) 12, 396. https://doi.org/10.3390/en12030396.

Van Gerven, T., Stankiewicz, A., 2009. Structure, Energy, Synergy, Time—The Fundamentals of Process Intensification. Ind. Eng. Chem. Res 48, 2465–2474. https://doi.org/10.1021/ie801501y.

Vesvikar, M.S., Al-Dahhan, M., 2005. Flow pattern visualization in a mimic anaerobic digester using CFD. Biotechnol. Bioeng. 89, 719–732. https://doi.org/10.1002/bit.20388.

Wang, J., Xue, Q., Guo, T., Mei, Z., Long, E., Wen, Q., Huang, W., Luo, T., Huang, R., 2018. A review on CFD simulating method for biogas fermentation material fluid. Renew. Sustain. Energy Rev. 97, 64–73. https://doi.org/10.1016/j.rser.2018.08.029.

Wei, P., Mudde, R.F., Uijttewaal, W., Spanjers, H., van Lier, J.B., de Kreuk, M., 2019. Characterising the two-phase flow and mixing performance in a gas-mixed anaerobic digester: Importance for scaled-up applications. Water Res 149, 86–97. https://doi.org/10.1016/j.watres.2018.10.077.

Wichterle, K., Kadlec, M., Žák, L., Mitschka, P., 1984. SHEAR RATES ON TURBINE IMPELLER BLADES. Chem. Eng. Commun. 26, 25–32. https://doi.org/10.1080/00986448408940200.